scientific reports

Check for updates

OPEN

Modeling treatment of diabetic wounds with oxygen therapy and senolytic drug

Nourridine Siewe[1]✉ & Avner Friedman[2]

Diabetic wounds are common in patients with type 2 diabetes; they are ischemic and inflammatory, and difficult to heal without intervention. Hyperbaric oxygen therapy (HBOT) is a standard treatment, but its effectiveness is limited to a subset of the aging population. Senescent fibroblasts, a hallmark of aging, impair wound healing, and senolytic drugs, like quercetin (*Q*), which target senescent cells, may improve healing. In this study, we developed a mathematical model that defines biological aging through two parameters, η and A_0, that decline with age. These parameters reflect the biological age of an individual, where η represents fibroblast proliferation and A_0 represents the production of the angiogenetic protein VEGF. Our model predicts that treatment with only HBOT achieves wound closure, within normal expectable time, for patients with a limited subset pairs of (η, A_0), and this subset is increased to a larger subset by combining *Q* with HBOT. The two subsets of (η, A_0) are determined explicitly by simulations of the model. To make these results applicable in clinical setting, one will have to relate the aging parameters η and A_0 to tangible marks of biological-aging factors.

The process of wound healing is divided into four overlapping stages: homeostasis, inflammatory, proliferation, and remodeling. In homeostasis, immediately after injury, platelets from damaged capillaries in the wound bed release PDGF, which stimulates resident fibroblasts[1], who are then attracted to the wound and begin to secrete PDGF[2]. Actually, neutrophils are one of the first cells that are recruited to the site of the wound. Their primary role is to prevent infection by attacking any microbe attempting to invade the body through the open skin wound[3]. For simplicity, we do not include in our model neutrophils and this very early phase of inflammation. In the inflammatory phase, blood monocytes are attracted to the wound microenvironment, where they differentiate into inflammatory macrophages M_1[4] that produce inflammatory cytokines, in particular TNF-α[5]. Fibroblasts secrete TGF-β[6], which induces polarization from M1 to anti-inflammatory M2 macrophages[7], and M2 macrophages secrete TGF-β[5]. TNF-α induces polarization from M2 to M1 macrophages[8]. In the proliferation phase, M2 macrophages and fibroblasts secrete VEGF[4,9], and VEGF promotes angiogenesis by stimulating proliferation of endothelial cells and the blood capillary system, thereby increasing the supply of oxygen to the cells in wound microenvironment[10] and enabling growth of tissue into the wound. Collagen deposition by fibroblasts, promoted by TGF-β[11], enables wound closure and end of the actual healing of the wound, except for wound remodeling. The fourth phase of wound remodeling and scar formation may take many months. Here we focus on the first three phases and on wound closure.

In normal dermal wound healing, the inflammatory phase takes at most one or two weeks, and wound closure takes weeks. Such wounds are called acute wounds. Wounds that do not heal in normal expectable time are called chronic wounds. Chronic wounds are consistently inflamed and may not heal without intervention. Chronic wounds include diabetic foot ulcer, ischemic wounds (arterial insufficiency), and pressure ulcer. Chronic wounds are more common in older rather than younger individuals[12,13]. Reviews of chronic wounds and potential therapies in adults are given in[12–15].

Cellular senescence is a permanent arrest of normal cell cycle, while maintaining cell viability. Senescent cells secrete senescence-associated secretory phenotype (SASP) which include variety of proteins. Cellular senescence is the primary hallmark of aging, but tissue disruption associated with cutaneous wounds also gives rise to senescent cells[16]. SASP of senesent fibroblasts secrete VEGF[17] and IL-6[18,19].

A review of cellular senescence in skin aging and age related pathologies, including dermal wounds, is given in[20]. The total number of fibroblasts is reduced by 35% in aged skin (>80 years) while the number of senescent fibroblasts is increased significantly with age[21,22]. Senescent fibroblasts in aging negatively affect dermal wound healing, and may lead to chronic wounds[23]. Senescent fibroblasts and macrophaes, exacerbate inflammation by secreting IL-6[14,19], which, in chronic wounds, enhance M2→M1 polarization[18,24]. The production of VEGF

[1]School of Mathematics and Statistics, Rochester Institute of Technology, Rochester, NY, USA. [2]Department of Mathematics, The Ohio State University, Columbus, OH, USA. ✉email: nxssma@rit.edu

by macrophages and fibroblasts in wound healing is reduced in aging[25] by cellular senescence[26], resulting in impaired angiogenesis[25,26].

In this paper we consider diabetic wounds: wounds that are more common in patients with diabetes type 2. Such wounds are consistently inflammatory. Indeed the rate of M_1/M_2 correlates with the degree of insulin resistance[27]. This means that the polarizations M1$\rightleftarrows$M2 are weighted toward M1, or that the normal transition from M1 to M2 is partially blocked.

Diabetic dermal wounds (e.g., diabetic foot ulcer) are ischemic, while the adaptive response to hypoxia is impaired in diabetes due to hyperglycemia[28]. Diabetic wounds are treated by oxygen therapy, either by topical wound therapy[29], or by hyperbaric oxygen therapy[30–32] where the patient spends several hours daily in the hyperbaric chamber where the oxygen pressure is three times the pressure in air.

Senolytic drugs (e.g., quercetin, dasatinib, fisetin) are drugs that eliminate senescent cells. Such drugs are currently under study in diseases that are exacerbated in aging patients. In the present paper we consider diabetic wounds treated by combination of hyperbaric oxygen therapy (HBOT) and quercetin (Q). Experimental studies report that quercetin improves wound healing[33] and wound closure[34].

In this paper, we develop an age-structured mathematical model for diabetic wounds, represented by a system of partial differential equations. We use this model to evaluate the effectiveness of combining Q with HBOT in improving wound closure in diabetic patients.

We conduct simulations to assess the percentage of wound closure in patients of various ages under treatment with HBOT alone, Q alone, and combination of Q and HBOT.

Here "age" is defined by two parameters, A_0 and η($0 \le A_0 \le 1,\ 0 \le \eta \le 1$), which are increasing with chronological age. We determine the set of points (η, A_0) where wound closure in normal expectable time can be achieved by combining Q with HBOT, but not by HBOT alone.

Mathematical model

The mathematical model is based on the network shown in Fig. 1, where the blue connections represent the network for acute wound healing, and the red connections represent the network for chronic wound healing. The blue connections in Fig. 1 exclude senescent cells and diabetes-related variables. In this case, we assume the wound heals in normal expectable time without any treatment. On the other hand, the red connections in Fig. 1 incorporate perturbations to the healing process caused by aging (senescent cells, denoted by F_s) and diabetes (denoted by B_1 and B_2), which contribute to the development of chronic wounds. Table 1 lists the variables of the model; densities and concentrations are all in units of g/cm^3.

The wound region is assumed to be a cylinder with an axis normal to the skin and, for simplicity, we consider only the two-dimensional circular cross-section (e.g., the base of the cylinder) as in Fig. 2, with time-varying boundary defined by $r = R(t)$. The partially healed tissue is the shell $R(t) \le r \le B$, while the shell $B \le r \le \Gamma$ represents normal healthy tissue. For simplicity, as in[36], we ignore the thickness for the wound and assume that the "flat" wound is radially symmetric, depending solely on (r, t). Throughout the healing process, the

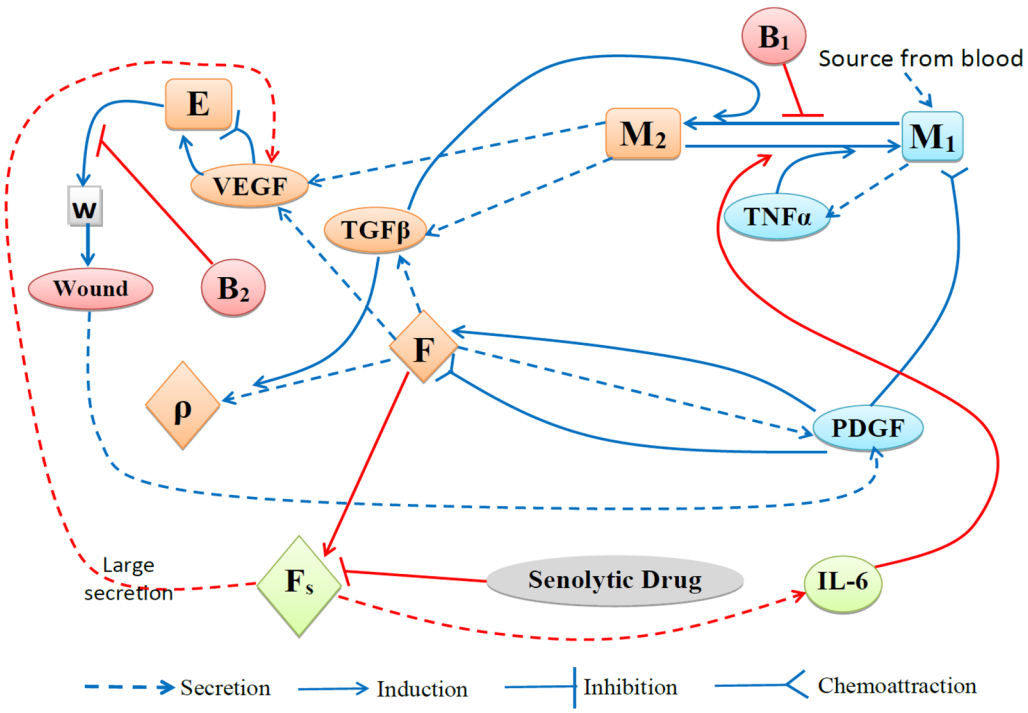

Fig. 1. Network of diabetic wound in aging. w=oxygen, E=endothelial cells, F=fibroblast, F_s=senescent fibroblast, ρ=ECM. B_1 and B_2 represent blockades in diabetic wounds.

Variables	Descriptions	Variables	Description
M_1	Density of M1 macrophages	M_2	Density of M2 macrophages
E	Density of endothelial cells	F	Density of fibroblasts
F_s	Density of senescent fibroblasts	ρ	Concentration of ECM
T_α	Concentration of TNF-α	T_β	Concentration of TGF-β
I_6	Concentration of IL-6	P	Concentration of PDGF
V	Concentration of VEGF	w	Concentration of oxygen

Table 1. Variables used in the model. Densities and concentrations are in units of g/cm^3.

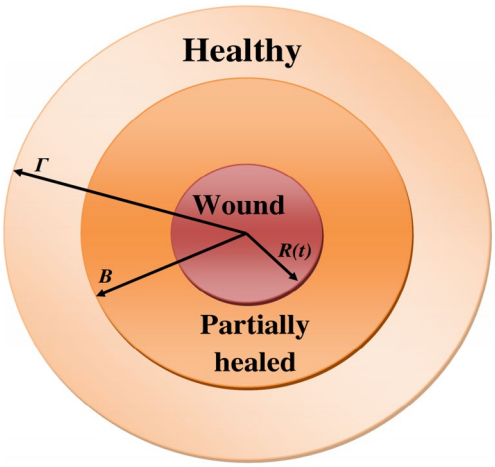

Fig. 2. Geometry around the wound. Wound area is $\{0 \le r \le R(t)\}$, partially healed area is $\{R(t) \le r \le B\}$, healthy area is $\{B \le r \le \Gamma\}$. This figure was reproduced from[35].

extracellular matrix (ECM) and its density ρ experience continuous movement with velocity $v = v(r,t)$, and that ρ is increasing.

To determine the velocity v, we adopt the approach outlined in[36], assuming that the partially healed tissue exhibits viscoelastic properties, which we model as a single-phase upper convected Maxwell fluid with pressure depending on its density: elastic over short timescales and viscous over longer ones. Given the slow dynamics of the healing process, we treat it as quasi-static. Letting Ψ represent the internal isotropic pressure associated with ρ in the partially healed medium, we use the following equation for v:

$$\frac{1}{r}\frac{\partial}{\partial r}\left(r\frac{\partial v}{\partial r}\right) - \frac{v}{r^2} = \frac{\partial \Psi}{\partial r},$$

where Ψ is defined as in[36] as follows:

$$\Psi = \begin{cases} 0, & \text{if } \rho \le \rho_1 \\ \gamma\left(\frac{\rho}{\rho_1} - 1\right), & \text{if } \rho > \rho_1 \end{cases} \tag{1}$$

for some positive parameters γ and ρ_1.

Fibroblasts and M2 macrophages are sensitive to hypoxia due to their dependence on oxidative phosphorylation, whereas M1 macrophages rely on glycolysis for respiration and are not affected by low oxygen levels[37,38]. Accordingly, we assume that the growth rates of fibroblasts F and M2 macrophages (but not M1 macrophages) are proportional to:

$$G(w) = \frac{w}{w_0 + w},$$

while the apoptotic death rate for these cells increases in proportion to:

$$D(w) = H(w_i - w),$$

where w_0 represents the oxygen concentration in healthy tissue, w_i denotes the oxygen level in extreme hypoxia, and $H(s)$ is defined as 0 if $s < 0$ and 1 if $s > 0$.

We assume that all cells within the partially healed tissue are moving with the same radial advection velocity v, and, in addition, they undergo diffusion. We can then write the dynamics of each species X of cells, in the partially healed tissue, in the following form:

$$\frac{\partial X}{\partial t}+\frac{1}{r}\frac{\partial}{\partial r}(rvX)-D_X\frac{1}{r}\frac{\partial}{\partial r}\left(r\frac{\partial X}{\partial r}\right)=F_X, \tag{2}$$

where D_X is the diffusion coefficient, and F_X represents the balance of the mass of X by the exchanges indicated in Fig. 1. We use the same structural equation for each cytokine X, but drop the advection velocity, since it is negligible compared to large diffusion coefficients of cytokines. An expression in F_X of the form $\lambda Z\frac{Y}{K_Y+Y}$ describes a process where species Y (e.g., proteins) is absorbed by cells Z at rate λ; K_Y is called the half-saturation of Y.

Equation for ECM (ρ)

Fibroblasts produce ECM proteins (e.g. collagen) in a process that is enhanced by TGF-β[11,35]. We assume that the ECM in the partially healed region is also undergoing advection with the velocity v, and write the equation for ρ as follows:

$$\frac{\partial \rho}{\partial t}+\frac{1}{r}\frac{\partial}{\partial r}(r\rho v)=\lambda_\rho F\left(1+\lambda_{\rho T_\beta}\frac{T_\beta}{K_{T_\beta}+T_\beta}\right)\left(1-\frac{\rho}{\rho_m}\right)-\mu_\rho\rho, \tag{3}$$

where ρ_m, the carrying capacity of ECM, is larger than ρ_1 in Eq. (1) and μ_ρ is the degradation rate of ρ.

Equations for M1 and M2 macrophages

We assume, as in[35], that there is a constant source of M1 macrophages from the blood to the wound, A_{M_1}, and a constant polarization from M1 to M2 macrophages (at rate $\lambda_{M_1M_2}$). According to Fig. 1, PDGF attracts and activates M1 macrophages[4], and TGF-β induces polarization from M1 to M2 macrophages[7]; and IL-6[18,24] and TNF-α[8] promote polarization of M2 to M1 macrophages. Hence M_1 satisfies the following equation:

$$\begin{aligned}\frac{\partial M_1}{\partial t}+\frac{1}{r}\frac{\partial}{\partial r}(rM_1v)-\frac{1}{r}\frac{\partial}{\partial r}\left[r\left(D_{M_1}\frac{\partial M_1}{\partial r}\right)\right]=\ & A_{M_1}-\frac{1}{r}\frac{\partial}{\partial r}\left[r\left(\chi_P M_1\frac{\partial P}{\partial r}\right)\right]\\ &+\lambda_{M_1P}M_1^0\frac{P}{K_P+P}-\lambda_{M_1M_2T_\beta}M_1\frac{T_\beta}{K_{T_\beta}+T_\beta}+\lambda_{M_2M_1T_\alpha}M_2\frac{T_\alpha}{K_{T_\alpha}+T_\alpha}\\ &-\frac{\lambda_{M_1M_2}}{1+B_1}M_1+\lambda_{M_2M_1I_6}M_2\frac{I_6}{K_{I_6}+I_6}-\mu_{M_1}M_1,\end{aligned} \tag{4}$$

where M_1^0 is a source of inactive M1 macrophages in the skin, μ_{M_1} is the death rate, and χ_P is the chemotactic coefficient of PDGF (P).

M2 macrophages are derived from the exchange M1→M2, their growth rate is proportional to $G(w)$, and their death rate increases due to a hypoxia. Hence,

$$\begin{aligned}\frac{\partial M_2}{\partial t}+\frac{1}{r}\frac{\partial}{\partial r}(rM_2v)-\frac{1}{r}\frac{\partial}{\partial r}\left[r\left(D_{M_2}\frac{\partial M_2}{\partial r}\right)\right]=&\frac{\lambda_{M_1M_2}}{1+B_1}M_1+\lambda_{M_1M_2T_\beta}G(w)M_1\frac{T_\beta}{K_{T_\beta}+T_\beta}\\ &-\lambda_{M_2M_1T_\alpha}M_2\frac{T_\alpha}{K_{T_\alpha}+T_\alpha}-\lambda_{M_2M_1I_6}M_2\frac{I_6}{K_{I_6}+I_6}-\mu_{M_2}M_2-\mu_{M_2w}D(w)M_2.\end{aligned} \tag{5}$$

Equation for fibroblasts (F) and senescent fibroblasts (F_s)

Fibroblasts are attracted to PDGF[2]. As in[35], we model their proliferation by a logistic growth model, with both proliferation and death rates being dependent on oxygen level. Fibroblasts can become senescent due to a variety of intracellular and extracellular stressors[16]. We assume a constant rate of senescent fibroblasts formation. In order to distinguish between old and young patients, we introduce a parameter $\eta\geq 0$ in that regulates the proliferation of senescent cells. Hence,

$$\begin{aligned}\frac{\partial F}{\partial t}+\frac{1}{r}\frac{\partial}{\partial r}(rFv)-\frac{1}{r}\frac{\partial}{\partial r}\left[r\left(D_F\frac{\partial F}{\partial r}\right)\right]=&-\frac{1}{r}\frac{\partial}{\partial r}\left[r\left(\chi_P F\frac{\partial P}{\partial r}\right)\right]+\lambda_F G(w)F\left(1-\frac{F}{F_m}\right)\\ &-\lambda_{FF_s}(1-\eta)F-\mu_F F-\mu_{Fw}D(w)F\end{aligned} \tag{6}$$

$$\frac{\partial F_s}{\partial t}+\frac{1}{r}\frac{\partial}{\partial r}(rF_sv)-\frac{1}{r}\frac{\partial}{\partial r}\left[r\left(D_{F_s}\frac{\partial F_s}{\partial r}\right)\right]=\lambda_{FF_s}(1-\eta)F-\mu_{F_s}F_s, \tag{7}$$

where, λ_{FF_s} and η are constants, and $0\leq\eta\leq 1$. The parameter η is decreasing with chronological age[16].

Equation for endothelial cells (E)

We assume a constant source (λ_E) of endothelial cells.

VEGF chemoattracts endothelial cells and stimulates their proliferation[10]. Hence E satisfies the following equation:

$$\frac{\partial E}{\partial t}+\frac{1}{r}\frac{\partial}{\partial r}(rEv)\ -\frac{1}{r}\frac{\partial}{\partial r}\left[r\left(D_E\frac{\partial E}{\partial r}\right)\right]=-\frac{1}{r}\frac{\partial}{\partial r}\left[r\left(\chi_V E\frac{\partial V}{\partial r}\right)\right]+\frac{\lambda_E}{1+B_2}\left(1+\lambda_{EV}\frac{V}{K_V+V}\right)-\mu_E E, \tag{8}$$

where χ_V is the chemotactic coefficient of V.

Equation for PDGF (P)

PDGF is released by damaged platelets from the wounds[39] and fibroblasts[2], and PDGF is depleted through chemoattracting F and M_1. We assume that the source of damaged platelets from the wound is proportional to the radius $R(t)$ of the wound. Hence PDGF satisfies the following equation:

$$\frac{\partial P}{\partial t}-\frac{1}{r}\frac{\partial}{\partial r}\left[r\left(D_P\frac{\partial P}{\partial r}\right)\right]=\lambda_P R(t)+\lambda_{FP}F-(\mu_{PF}F+\mu_{PM}M_1)\frac{P}{K_P+P}-\mu_P P, \tag{9}$$

where μ_P is the degradation rate of P and λ_P is constant in chronic wounds.

Equation for TNF-α (T_α)

TNF-α is produced by M1 macrophages[5], hence

$$\frac{\partial T_\alpha}{\partial t}-\frac{1}{r}\frac{\partial}{\partial r}\left[r\left(D_{T_\alpha}\frac{\partial T_\alpha}{\partial r}\right)\right]=\lambda_{M_1T_\alpha}M_1-\mu_{T_\alpha}T_\alpha, \tag{10}$$

where μ_{T_α} is the degradation rate of T_α.

Equation for TGF-β (T_β)

TGF-β is produced by fibroblasts and M2 macrophages[6], so that

$$\frac{\partial T_\beta}{\partial t}-\frac{1}{r}\frac{\partial}{\partial r}\left[r\left(D_{T_\beta}\frac{\partial T_\beta}{\partial r}\right)\right]=\lambda_{FT_\beta}F+\lambda_{M_2T_\beta}M_2-\mu_{T_\beta}T_\beta. \tag{11}$$

Equation for IL-6 (I_6)

IL-6 is secreted by senescent fibroblasts[18,19], so that

$$\frac{\partial I_6}{\partial t}-\frac{1}{r}\frac{\partial}{\partial r}\left[r\left(D_{I_6}\frac{\partial I_6}{\partial r}\right)\right]=\lambda_{F_sI_6}F_s-\mu_{I_6}I_6. \tag{12}$$

Equation for VEGF (V)

VEGF is produced by fibroblasts[9], senescent fibroblasts[17,40,41] and M2 macrophages[4,9]. The senescent fibroblasts secrete more VEGF than their presenescent counterparts[40,41]. However, in diabetic wounds of old people, VEGF production is decreased by both F and F_s[25]. VEGF is also depleted when it combines with receptors on endothelial cells. Hence,

$$\frac{\partial V}{\partial t}-\frac{1}{r}\frac{\partial}{\partial r}\left[r\left(D_V\frac{\partial V}{\partial r}\right)\right]=(\lambda_{FV}F+\lambda_{F_sV}F_s)A(t)+\lambda_{M_2V}M_2-\mu_{EV}E\frac{V}{K_V+V}-\mu_V V \tag{13}$$

where $A(t)$ is a decreasing function in t. We take

$$A(t)=\frac{A_0}{1+t^2/T_w^2},\qquad 0\le A_0\le 1, \tag{14}$$

where A_0 and T_w are a constants. The parameter A_0 is decreasing with chronological age.

Equation for oxygen (w)

Hence, w satisfies the following equation: We identify the density of blood vessel by E. Hence oxygen is increased proportionally to E, and is utilized by fibroblasts and M2 macrophages[35]. Hence,

$$\frac{\partial w}{\partial t}-\frac{1}{r}\frac{\partial}{\partial r}\left[r\left(D_w\frac{\partial w}{\partial r}\right)\right]=\lambda_{Ew}E-c_w(F+M_2)w. \tag{15}$$

Boundary conditions

We take the boundary conditions at $r=B$ to be the average serum concentration of the variables in diabetes type 2:

$$\begin{aligned}&M_1=M_1^0,\ M_2=M_2^0,\ F=F_0,\ F_s=F_s^0,\ E=E_0,\ w=w_0,\\&I_6=I_6^0,\ P=P_0,\ T_\alpha=T_\alpha^0,\ T_\beta=T_\beta^0,\ V=V_0,\end{aligned} \tag{16}$$

On the free boundary $r=R(t)$ we prescribe the following conditions:

$$
\begin{aligned}
&D_{M_1}\frac{\partial M_1}{\partial r}-\chi_P M_1\frac{\partial P}{\partial r}=0, \qquad \frac{\partial M_2}{\partial r}=0,\\
&D_F\frac{\partial F}{\partial r}-\chi_P F\frac{\partial P}{\partial r}=0, \quad D_E\frac{\partial E}{\partial r}-\chi_V E\frac{\partial V}{\partial r}=0, \quad -\frac{\partial P}{\partial r}=\beta_P R(t),\\
&\frac{\partial X}{\partial r}=0 \text{ for } F_s,\ I_6,\ T_\alpha,\ T_\beta,\ V,\ w.
\end{aligned}
\tag{17}
$$

Note that in Eq. (17) all species, except P, satisfy no-flux condition, while there is an influx of P from the wound, proportional to the size of the wound.

The partially healed area has a fixed boundary $r = B$ and a boundary $r = R(t)$ that moves in response to the pressure Ψ. Accordingly, we take

$$v = 0 \text{ at } r = B, \tag{18}$$

$$\frac{\partial v}{\partial r} = \Psi \text{ at } r = R(t). \tag{19}$$

We assume that the wound boundary $r = R(t)$ decreases with the velocity v of the ECM, that is

$$\frac{dR}{dt} = v(R(t), t); \tag{20}$$

v is expected to have negative values.

Initial conditions

We take $R(0) = 1$ cm, $B = 1.5$ cm, and initial conditions for $R(0) \le r \le B$ as follows:

$$
\begin{aligned}
&v(r,0)=0,\ \rho(r,0)=\rho_0,\ P(r,0)=\beta_P R(0)(B-r)+P_0\left(\frac{r-R(0)}{B-R(0)}\right)^2,\\
&X(r,0)=X_0\left(\frac{r-R(0)}{B-R(0)}\right)^2,
\end{aligned}
\tag{21}
$$

for all other species, where X_0 is the steady state value as in (16) and ρ_0 is the dry weight of tissue.

Since the level of senescent cells depends on the age of the patient, we take

$$F_s(0) = F_s^0(1-\eta), \tag{22}$$

where F_s^0 represents the level of F_s for the oldest patient (with $\eta = 0$).

Note that the initial conditions are consistent with the boundary conditions at $r = R(0)$ and $r = B$.

Simulations and results

All the computations were done using Python 3.7.3. The parameter values of the model equations are estimated in Section 7 and are listed in the Table 4. We introduce the percent of wound closure (PWC) by the formula

$$\text{PWC}(t) = \frac{R(0) - R(t)}{R(0)} \times 100\%. \tag{23}$$

Diabetic wounds without senolytics

In the sequel we define "age" by the two parameters, A_0 and η, which are decreasing when the chronological age (t) increases. In particular, a person with (η_1, A_{01}) is older than a person with (η_2, A_{02}) if $\eta_1 < \eta_2$ and $A_{01} < A_{02}$.

In Fig. 3 we show all the model variables and display the percent of wound closure at day 30 in the no drug case, for the oldest patient and a younger patient. The percentage of wound closure after 30 days is 5.1% in the oldest patient, and 6.7% in the younger patient. In both cases, as expected, the pro-inflammatory M_1 increases and tends to stabilize at a high value, while the anti-inflammatory M_2 continues to decrease. The oxygen level initially increases but then decreases due to the hypoxia-driven effects of diabetes. The level of senescent fibroblasts, denoted as F_s, increases monotonically with age in both the youngest and oldest patients, but the F_s level in the youngest patients remains lower than in the oldest patients. In each case, the level of IL-6 follows the trends observed for F_s.

It is interesting to note that whereas VEGF increases to 10×10^{-6} g/cm^3 in young patients, in old patients it increases to only 0.8×10^{-6} g/cm^3. F is also smaller in old compared to young patients, and so is M_2.

Simulations with drugs

Quercetin

Senolytics, such as quercetin and fisetin, are currently undergoing clinical trials for various diseases like idiopathic pulmonary fibrosis, chronic kidney disease, Alzheimer's disease, and diabetes[42]. However, there have been no clinical trials to date exploring their effectiveness in wound healing.

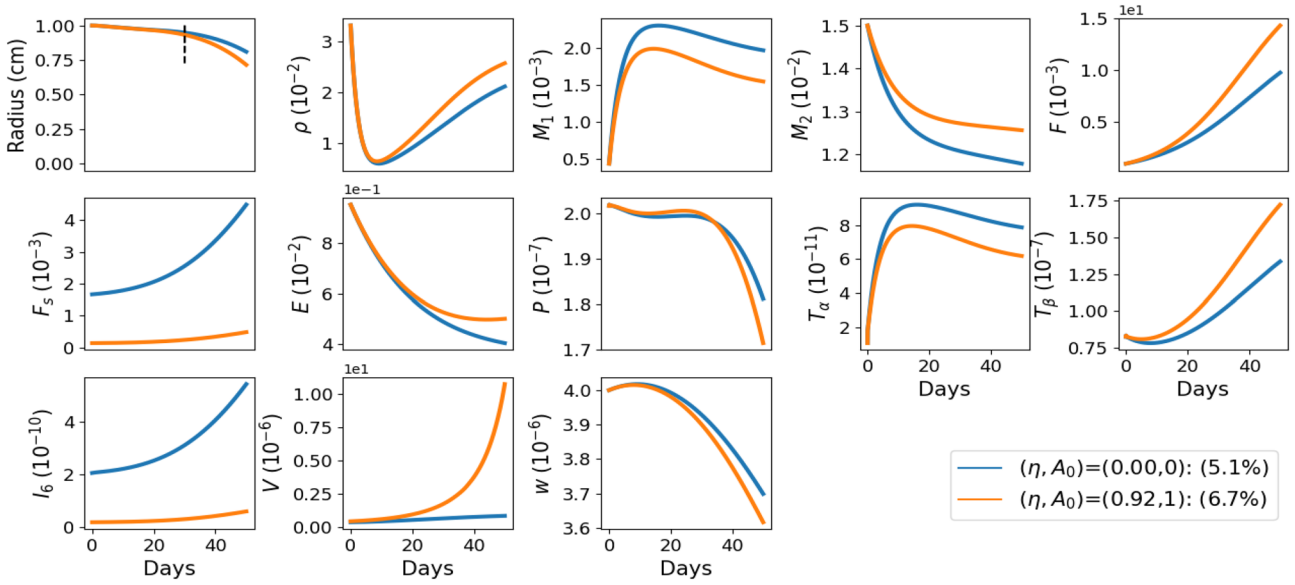

Fig. 3. Simulations of all the model variables in oldest patient ($(\eta, A_0) = (0, 0)$), and younger patient ($(\eta, A_0) = (0.92, 1)$), with no drug. All the variables are in units of g/cm^3.

Quercetin, a natural supplement, is known to promote wound healing by enhancing the proliferation and migration of fibroblasts[43] and by eliminating senescent cells[44]. Quercetin also enhances ECM production[13,45]. In combination with dasatinib, a tyrosine kinase inhibitor that triggers apoptosis in senescent cells[46], quercetin has been shown to significantly reduce the burden of senescent cells across multiple tissues in human studies[46–48].

Cutaneous wounds were treated with quercetin in mice (*in vivo*)[49,50] and in humans (*in vitro*)[34]. In all these cases, subjects given the senolytic drugs exhibited faster wound healing compared to the control groups.

We simulate the senolytic drug quercetin, and denote it by Q. We accordingly update Eqs. (3), (6) and (7) as follows:

$$\frac{\partial \rho}{\partial t} + \frac{1}{r}\frac{\partial}{\partial r}(r\rho v) = \lambda_\rho F\left(1 + \lambda_{\rho T_\beta}\frac{T_\beta}{K_{T_\beta} + T_\beta}\right)\left(1 - \frac{\rho}{\rho_m}\right)(1 + \mu_{\rho Q}Q) - \mu_\rho \rho, \tag{24}$$

$$\begin{aligned}\frac{\partial F}{\partial t} + \frac{1}{r}\frac{\partial}{\partial r}(rFv) - \frac{1}{r}\frac{\partial}{\partial r}\left[r\left(D_F\frac{\partial F}{\partial r}\right)\right] &= -\frac{1}{r}\frac{\partial}{\partial r}\left[r\left(\chi_P F\frac{\partial P}{\partial r}\right)\right] \\ &+ \lambda_F G(w)(1 + \lambda_{FQ}Q)F\left(1 - \frac{F}{F_m}\right) - \lambda_{FF_s}(1-\eta)F - \mu_F F - \mu_{Fw}D(w)F\end{aligned} \tag{25}$$

$$\frac{\partial F_s}{\partial t} + \frac{1}{r}\frac{\partial}{\partial r}(rF_s v) - \frac{1}{r}\frac{\partial}{\partial r}\left[r\left(D_{F_s}\frac{\partial F_s}{\partial r}\right)\right] = \lambda_{FF_s}(1-\eta)F - \mu_{F_s}F_s - \mu_{F_sQ}QF_s, \tag{26}$$

where $\mu_{\rho Q}$, λ_{FQ} and μ_{F_sQ} are constants.

Quercetin is given in pills daily. At 1 g/d it can be given safely (from damage to the liver) for up to 12 weeks. The half-life of quercetin is 15–28h, so by approximation we take it as a constant: $Q = 1$ g/d and accordingly estimate the parameters λ_{FQ} and μ_{F_sQ}.

Oxygen therapy

In hyperbaric oxygen therapy (HBOT) chamber, the oxygen pressure is three times the pressure in air, and the patient remains in the chamber for, typically, 2 hours daily. We represent this treatment in our model by including in Eq. (15) a (constant) source of oxygen, as shown in the following modified equation:

$$\frac{\partial w}{\partial t} - \frac{1}{r}\frac{\partial}{\partial r}\left[r\left(D_w\frac{\partial w}{\partial r}\right)\right] = \lambda_{Ew}E - c_w(F + M_2)w + \gamma_w h(t), \tag{27}$$

where

$$h(t) = \begin{cases} 1, & \text{for two hours every day,} \\ 0, & \text{otherwise,} \end{cases}$$

and $\gamma_w > 0$ is the dose of oxygen administered between 12:00–14:00 every day. We also change the boundary condition for w on $r = B$, increasing w_0 by $\int^t \gamma_w(s)ds$ during the hours between 12:00–14:00.

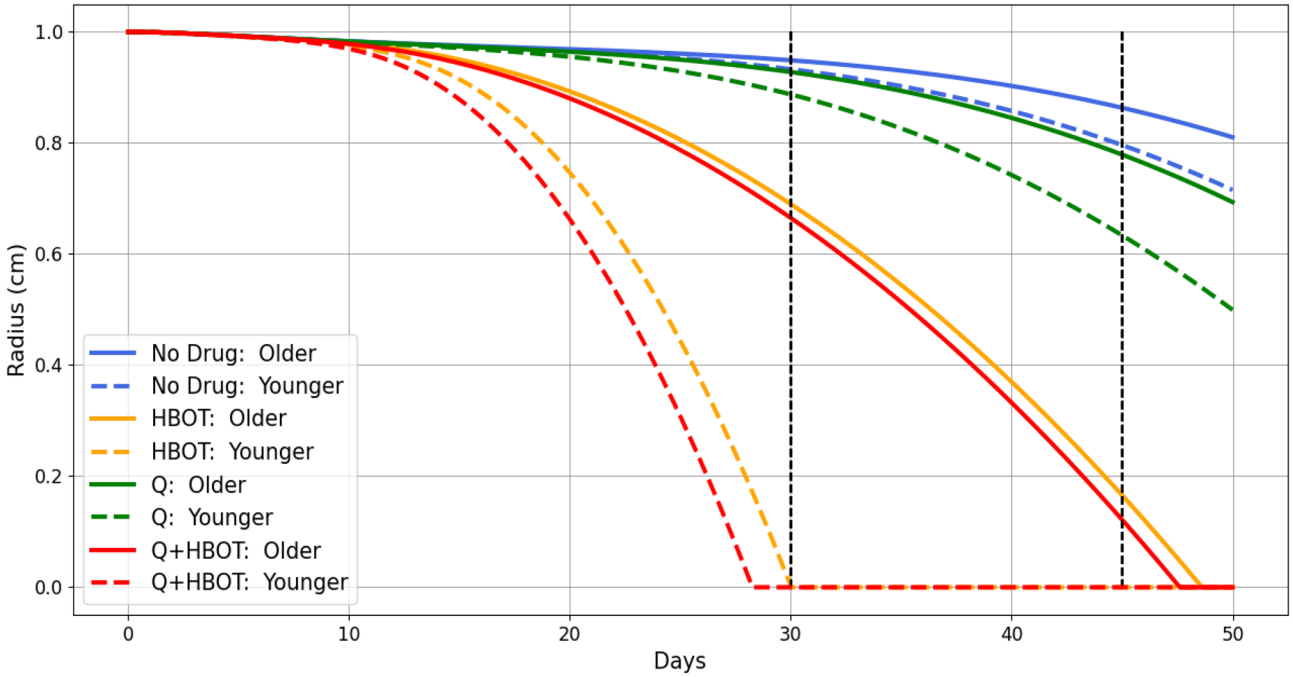

Fig. 4. Diabetic wound treatment with HBOT and quercetin: Simulations of the wound radius with various combinations of hyperbaric oxygen therapy (HBOT) and quercetin (Q) for the youngest patient $(\eta, A_0) = (0.92, 1)$ and the oldest patient $(\eta, A_0) = (0, 0)$. The percentages represent the percent of wound closure (PWC) of the respective treatments at day 30; we mark day 30 and day 45.

Patients (η, A_0)	1 (0.15,0.56)	2 (0.3,0.67)	3 (0.6,0.78)	4 (0.7,0.89)	5 Youngest (0.92,1)
No Drug (%)	5.41	5.67	6.17	6.35	6.71
HBOT (%)	82.29	90.26	96.12	97.48	99.55
Q (%)	7.89	8.53	9.82	10.28	11.24
HBOT+Q (%)	92.56	100	100	100	100

Table 2. Percent of wound closure (PWC) at day 30 in patients of various ages under treatment with hyperbaric oxygen therapy (HBOT) and quercetin (Q). The daily dose of quercetin is 1.0 g, and $\gamma_w = 1.2 \times 10^{-6}$ g/cm^{3}d^{-1}.

Treatment with HBOT and quercetin

In Fig. 4, we show the profiles of the wound radius (R) for 50 days, for two patients of extreme age difference (Younger with $(\eta, A_0) = (0.92, 1)$ and Older with $(\eta, A_0) = (0, 0)$), both with and without drugs HBOT and Q. The profiles for the no-drug case are similar to those in Fig. 3.

Without treatment, diabetic wounds do not close (PWC in 5.1%–6.7%). When using Q alone, there is only a mild improvement in the PWC (between 7.2%–11.2%) compared to the case with no drug.

For younger patients, HBOT treatment does not result in complete wound closure within the expectable 30 days (PWC=99.6%); but when Q is combined with HBOT, complete wound closure is achieved. Older patients, on the other hand, require additional time for complete wound closure.

We can use the model to depict cases where complete wound closure can be achieved with Q+HBOT therapy, but not with HBOT alone. Table 2 presents the 30-day PWC for 5 patients, listed in order of decreasing age. In all cases, treatment with only Q does not significantly improve wound closure. Treatment with only HBOT significantly improves PWC but does not fully close the wound. Combining Q with HBOT results in complete wound closure, except for the oldest patient ($(\eta, A_0) = (0.15, 0.56)$).

In Table 3, we consider 5 patients older than those in Table 2, and show their PWC after 45 days of treatment. As in Table 2. Treatment with only Q does not result in significant wound closure. Under HBOT alone, the youngest patient (#10, $(\eta, A_0) = (0.03, 0.44)$) achieves complete wound closure. The next two older patients (#8 and #9) achieve wound closure only when Q is combined with HBOT. However, the oldest patients (#6 and #7) do not achieve wound closure with HBOT+Q.

Figure 5A is a color map of PWC(30) under treatment with HBOT, and Fig. 5B is a color map under treatment with Q+HBOT, where on the horizontal axis, A_0 reflects how well the organism performs angiogenesis functions,

Patients (η, A_0)	6 (Oldest) (0,0)	7 (0.001,0.11)	8 (0.003,0.22)	9 (0.004,0.33)	10 (0.03,0.44)
No Drug (%)	13.66	13.72	13.79	13.86	14.11
HBOT (%)	83.41	87.63	95.62	99.47	100
Q (%)	22.09	22.16	22.25	22.33	22.8
HBOT+Q (%)	87.81	92.3	100	100	100

Table 3. Percent of wound closure (PWC) at day 45 in patients of various ages under treatment with hyperbaric oxygen therapy (HBOT) and quercetin (Q). The daily dose of quercetin is 1.0 g, and $\gamma_w = 1.2 \times 10^{-6}$ g/cm^{3}d^{-1}.

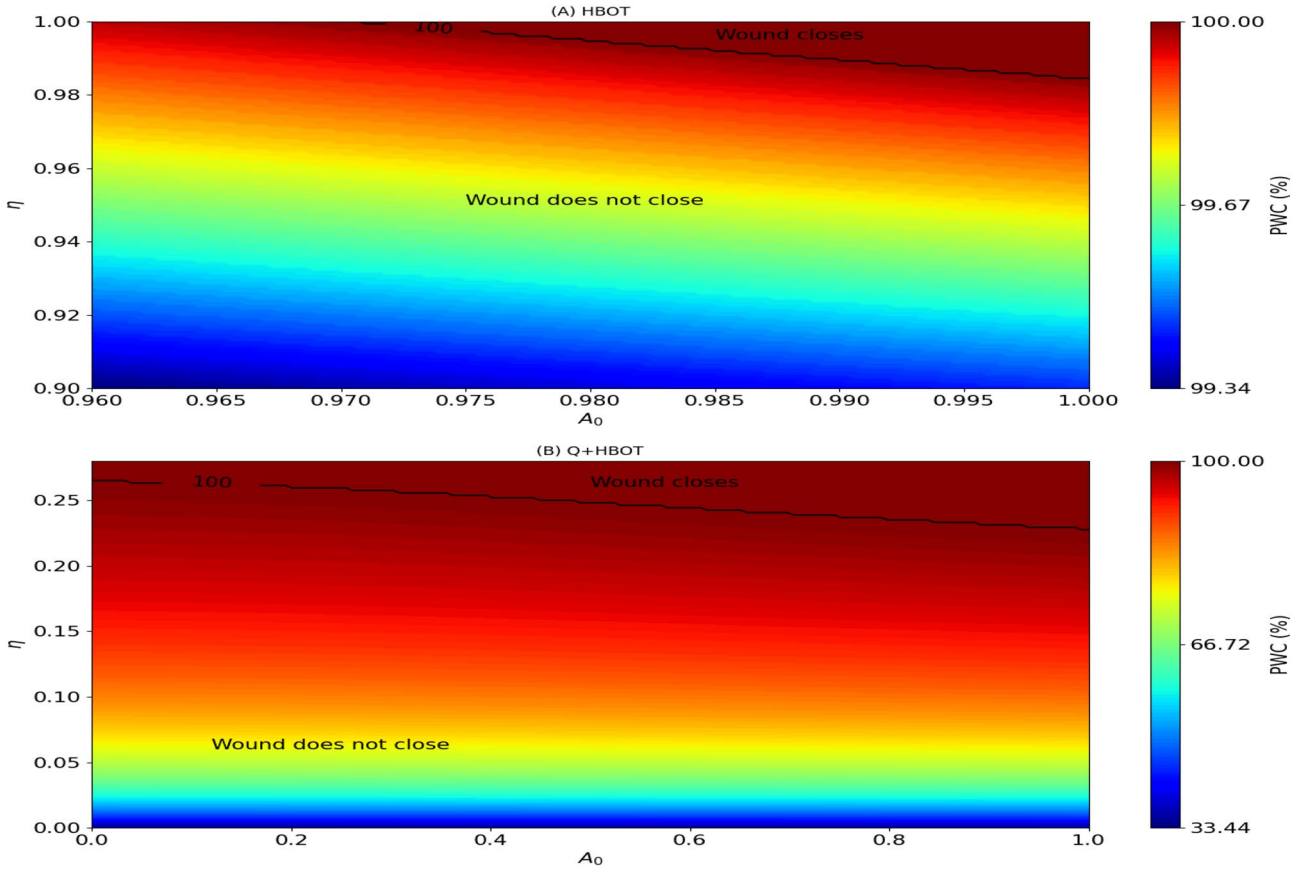

Fig. 5. Effect of age (η, A_0) on percent wound closure: Simulations of PWC(30) under HBOT (**A**) and Q+HBOT (**B**) as the pair (η, A_0) vary; note the ranges for η and A_0 in each plot. The black curves represent the values of (η, A_0) where PWC(30)$= 100\%$. The black curves represent the pairs (η, A_0) where PWC(30)=100%.

and on the vertical axis, η represents the proliferation of senescent cells. The range of (η, A_0) was restricted in order to display, more clearly, in each of the figures, the region where PWC(30)$= 100\%$.

Based on Fig. 5, Figure 6 shows the region in the (η, A_0) plane where treatment with HBOT does not achieve wound closure in 30 days, but treatment with Q+HBOT does. This region lies between two equi-PWC curves: The upper curve includes the extreme points (1, 0.97) and (0.986, 1), and the lower once includes the extreme points (0.265, 0) and (0.236, 1).

Discussion

Diabetic wounds represent a growing global health crisis, with approximately 15-25% of diabetic patients developing chronic foot ulcers that frequently lead to infections and amputations[51]. Current treatment modalities include advanced wound dressings, negative pressure therapy, hyperbaric oxygen therapy (HBOT), and emerging biologic therapies, but these approaches often fail to address the underlying pathophysiology of impaired healing in diabetic patients[52]. The economic burden is staggering, with annual U.S. costs ranging between $9 to $13 billion due to prolonged hospitalizations, frequent debridements, and high recurrence rates; in addition to the

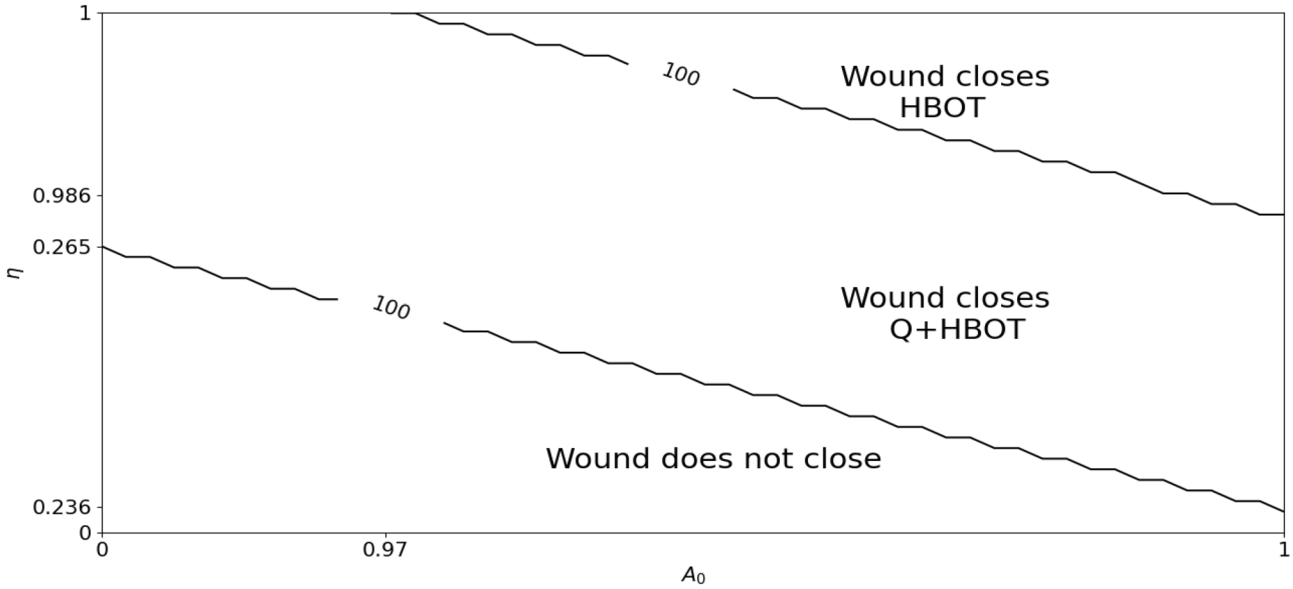

Fig. 6. Effect of age (η, A_0) on percent wound closure: Simulations PWC(30) under HBOT and Q+HBOT as the pair (η, A_0) vary. The region between the two curves represents the ages (η, A_0) under which wound closure is achieved under treatment with Q+HBOT, but not under treatment with HBOT alone.

cost for management of diabetes mellitus alone[53,54]. These costs are significantly lower in European systems like England's NHS and France's universal healthcare, where standardized treatment protocols, preventive care models, and price controls reduce both complication rates and expenditures[55,56]. The medical community in the U.S. has proposed several cost-reduction strategies, including value-based care models, early screening programs, and the adoption of senolytic therapies to target cellular senescence – a key contributor to impaired wound healing[57]. However, significant obstacles remain, including fragmented healthcare delivery, inconsistent insurance coverage, and a lack of reliable biomarkers to predict treatment response.

This paper contributes to addressing these challenges by developing a mathematical model that quantifies biological aging through two key parameters (η for fibroblast proliferation and A_0 for VEGF production) to predict patient responsiveness to HBOT and senolytic therapy with quercetin (Q). Our simulations demonstrate that while HBOT alone is effective only for a limited subset of patients with specific (η, A_0) values, combining HBOT with Q expands the treatable population by addressing cellular senescence[16]. This approach could reduce costs by enabling clinicians to: (1) avoid ineffective HBOT in non-responders, (2) identify patients who would benefit from adjunct senolytic therapy, and (3) potentially shorten treatment duration through targeted interventions. While the model requires clinical validation to correlate η and A_0 with measurable biomarkers, it provides a quantitative framework for personalized treatment decisions that could optimize resource allocation in diabetic wound care[58].

Conclusion

Cellular senescence is a permanent arrest of cell cycle while maintaining viability. Cellular senescence is the hallmark of aging. Senescent cells secrete proteins that have negative effect on tissue regeneration. Diabetic wounds, wounds that develop in individuals with type 2 diabetes, tend to be ischemic due to the inflammation induced by the diabetic condition. And in aging individuals with diabetes type 2, due to also cellular senescence of fibroblasts, diabetic wounds are more likely to become chronic wounds.

Ischemic wounds are commonly treated with oxygen infusion, where the patient spends several hours per day in hyperbaric oxygen therapy chamber (HBOT) under oxygen pressure three times the pressure in air. Senolytic drugs that eliminate senescent cells, such as quercetin (Q), are currently used in experimental studies in chronic wounds. In this paper we simulate treatments with HBOT and Q, separately or in combination, of diabetic wounds in aging population.

To better understand the impact of aging on wound healing, we developed a predictive mathematical model that defines an individual's biological age using two key parameters: η and A_0. These parameters decrease with chronological age, where $0 \leq \eta \leq 1$ and $0 \leq A_0 \leq 1$. The parameter η reflects age-related changes in the proliferation of senescent cells, while A_0 represents age-related production of the angiogenetic protein VEGF. Lower values of η and A_0 indicate a biologically older individual. Our model can be used to predict the profile of the open-wound radius, with or without treatment, for any biological-age pair (η, A_0).

We simulated the threshold of two (η, A_0)-sets, S_1 and S_2($S_1 \subset S_2$): patients in S_1 achieve wound closure (in expectable time of 30 days) if treated with HBOT, and patients in S_2 achieve ful wound closure when treated with Q+HBOT. We conclude that for the biologically-old patients in $S_2 - S_1$, to achieve wound closure they need to be treated with combination of the senolytic drug and HBOT; HBOT alone will not yield wound closure.

The limitation of the model is that it is unable to precisely associate the biological-age parameters (η, A_0) to any tangible marks that can be determined and measured for each individual. For this reason, the predictions of the model, at present, are highly qualitative.

Future studies should aim to determine the dependence of η and A_0 on factors such as lifestyle, general health, and body mass to further personalize treatment strategies. This would significantly improve the predictive accuracy of our model and allow for more individualized care. Ultimately, the integration of these parameters into clinical practice could significantly improve the management of chronic wounds in the aging diabetic population, providing clinicians with a tool to better predict healing outcomes and optimize treatment plans.

Parameters sensitivity analysis

We performed global sensitivity analyses (see Fig. 7). The output was the percent wound closure at day 30 (PWC), and the p-values for all the parameters were less than 10^{-8}. The computations were done using Latin Hypercube Sampling/Partial Rank Correlation Coefficient (LHS/PRCC) with a Matlab package by[59,60], with the parameters listed λ_ρ, λ_{M_1P}, $\lambda_{M_1M_2T_\beta}$, $\lambda_{M_2M_1T_\alpha}$, $\lambda_{M_1M_2}$, $\lambda_{M_2M_1I_6}$, λ_F, λ_{FF_s}, λ_E, λ_{EV}, λ_{FP}, $\lambda_{M_1T_\alpha}$, λ_{FT_β}, $\lambda_{F_sI_6}$, λ_{FV} and λ_{F_sV} in Table 4.

The ranges for the parameters were between $\pm 50\%$ of their baselines in Table 4, except λ_ρ whose range was between $\pm 10\%$ of its baseline in Table 4.

Figure 7 shows that λ_ρ and λ_F are the most positive correlated parameters, with $\lambda_{M_1M_2T_\beta}$, λ_{FT_β} and λ_{F_sV} also showing significant positive correlations. The parameter λ_ρ represents the rate of ECM production; as it increases, ECM production rises, leading to a reduction in wound size and an increase in PWC. Similarly, an increase in λ_F, which denotes the rate of fibroblast proliferation, results in enhanced ECM production and a larger PWC. Additionally, increases in the parameters $\lambda_{M_1M_2T_\beta}$ and λ_{FT_β} promote the $M_1 \to M_2$ polarization, further contributing to increased ECM production and larger PWC. An increase in λ_{F_sV} leads to an increase in V, which in turn results in an increase in E. This implies that w also increases, thereby enhancing the wound healing process. Note that the positive correlation of λ_{FV} is smaller than the positive correlation of λ_{F_sV}; this is because λ_{FV} is 10 times smaller than λ_{F_sV}.

The reverse is true for the parameters $\lambda_{M_2M_1I_6}$, $\lambda_{M_2M_1T_\alpha}$ and $\lambda_{M_1T_\alpha}$, which are the most negatively correlated parameters. As $\lambda_{M_2M_1I_6}$ and $\lambda_{M_2M_1T_\alpha}$ increase, the density of M1 macrophages also increases, which decreases PWC. An increase in $\lambda_{M_1T_\alpha}$ leads to higher levels of TNF-α, which similarly results in an increase in M1 macrophages, and decrease PWC.

All other parameters have small correlations, and their positive or negative correlation can easily be inferred from the model equations. For instance, increase in any parameter that results in increase $M_1 \to M_2$ will improve healing and hence increase PWC, and is positively correlated.

Parameter estimations

We assume that in steady-state, $\frac{X}{K_X+X} = \frac{1}{2}$, or $X = K_X$ for any protein species, X, where K_X is the half-saturation of X.

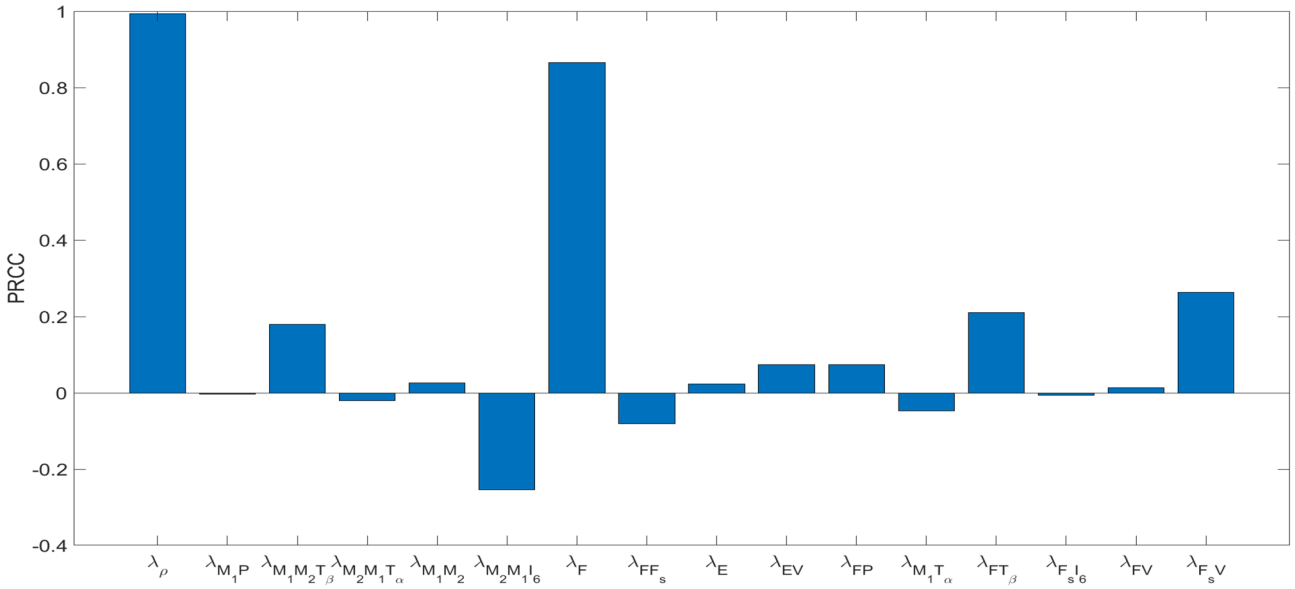

Fig. 7. LHS–PRCC sensitivity analysis of radius reduction at day 30. The horizontal axis lists the parameters and the vertical axis represents the PRCC index. The samplings are done with $\pm 50\%$ of the baselines for the parameters as in Tables 4, except for λ_ρ whose range is $\pm 10\%$ of the baseline.

Parameters	Descriptions	Values	References
λ_ρ	Rate of production of ECM by F	21.71 d^{-1}	est.
λ_{M_1P}	Rate of recruitment of M_1	$6.6 \times 10^{-3}\mathrm{d}^{-1}$	est.
$\lambda_{M_1M_2T_\beta}$	Rate of T_β-induced transition $M_1 \to M_2$	$6.53 \times 10^{-2}\mathrm{d}^{-1}$	est.
$\lambda_{M_2M_1T_\alpha}$	Rate of T_α-induced transition $M_2 \to M_1$	$5.94 \times 10^{-3}\mathrm{d}^{-1}$	est.
$\lambda_{M_2M_1I_6}$	Rate of I_6-induced transition $M_2 \to M_1$	$5.94 \times 10^{-3}\mathrm{d}^{-1}$	est.
$\lambda_{M_1M_2}$	Rate of transition $M_1 \to M_2$	$3.3 \times 10^{-4}\mathrm{d}^{-1}$	est.
λ_F	Rate of proliferation of F	0.15 d^{-1}	est.
λ_{FF_s}	Rate of transition $F \to F_s$	0.015 d^{-1}	est.
λ_E	Rate of maturation of E by EPC	$3 \times 10^{-4}\mathrm{d}^{-1}$	est.
λ_P	Recruitment rate of P	1.19×10^{-4} $\mathrm{g/cm^2 d^{-1}}$	est.
λ_{FP}	Rate of production of P by F	$7 \times 10^{-5}\mathrm{d}^{-1}$	est.
$\lambda_{M_1T_\alpha}$	Rate of production of T_α	$8.664 \times 10^{-6}\mathrm{d}^{-1}$	est.
λ_{FT_β}	Rate of production of T_β by F	$2.5 \times 10^{-3}\mathrm{d}^{-1}$	est.
$\lambda_{M_2T_\beta}$	Rate of production of T_β by M_2	$2.5 \times 10^{-3}\mathrm{d}^{-1}$	est.
$\lambda_{\rho T_\beta}$	T_β-factor of ρ-production by F	0.1	est.
λ_{M_2V}	Rate of production of V by M_2	3.17 d^{-1}	est.
λ_{FV}	Rate of production of V by F	3.17 d^{-1}	[40,41]est.
λ_{F_sV}	Rate of production of V by F_s	31.7 d^{-1}	[40,41]est.
$\lambda_{F_sI_6}$	Rate of production of I_6 by F_s	$2.9343 \times 10^{-7}\mathrm{d}^{-1}$	[66]est.
λ_{Ew}	Rate of circulation of oxygen	$2.4 \times 10^{-6}\mathrm{d}^{-1}$	est.
λ_{FQ}	Rate of Q-enhanced proliferation of F	0.2 $\mathrm{d\,g^{-1}}$	est.
c_w	Rate of consumption of oxygen	0.3 $\mathrm{cm^3/g\,d^{-1}}$	est.
γ	Factor of internal isotropic medium	0.19 d^{-1}	est.
χ_P	Chemotactic coefficient of P	1000 $\mathrm{cm^5/g\ d}$	[81]est.
χ_V	Chemotactic coefficient of V	1000 $\mathrm{cm^5/g\ d}$	[81]est.
$\lambda_{\rho T_\beta}$	Fraction of effect of T_β on production of ρ by F	0.1	est.
λ_{EV}	Coefficient of maturation of E by V	1	est.
K_{T_β}	Half-saturation of T_β	10^{-7} $\mathrm{g/cm^3}$	[70]est.
K_{I_6}	Half-saturation of I_6	4.102×10^{-10} $\mathrm{g/cm^3}$	[69]est.
K_P	Half-saturation of P	4×10^{-6} $\mathrm{g/cm^3}$	[71]est.
K_{T_α}	Half-saturation of T_α	10^{-10} $\mathrm{g/cm^3}$	[72]est.
K_V	Half-saturation of V	1.15×10^{-6} $\mathrm{g/cm^3}$	[9]est.
ρ_0	Healthy state of ECM	0.04 $\mathrm{g/cm^3}$	[61]est.
ρ_1	Threshold of pressure of ECM	0.008 $\mathrm{g/cm^3}$	[61]est.
ρ_m	Carrying capacity of ECM	0.044 $\mathrm{g/cm^3}$	[61]est.
A_{M_1}	Recruitment rate of M_1	7.5×10^{-5} $\mathrm{g/cm^3 d^{-1}}$	est.
w_0	Oxygen concentration	4×10^{-6} $\mathrm{g/cm^3}$	[82,83]est.
w_i	Oxygen concentration in extreme hypoxia	2.5×10^{-6} $\mathrm{g/cm^3}$	[82,83]est.
M_1^0	Steady state in health of M_1	2.5×10^{-3} $\mathrm{g/cm^3}$	[63]est.
M_2^0	Steady state in health of M_1	1.25×10^{-2} $\mathrm{g/cm^3}$	[63]est.
F_0	Steady state in health of F	7.5×10^{-3} $\mathrm{g/cm^3}$	[64,65]est.
F_s^0	Steady state in health of F_s	1.5×10^{-3} $\mathrm{g/cm^3}$	[66]est.
E_0	Steady state in health of E	10^{-2} $\mathrm{g/cm^3}$	[67,68]est.
μ_ρ	Degradation rate of ECM	0.37 d^{-1}	[36]
μ_P	Degradation rate of PDGF	33 d^{-1}	[84]est.
μ_{T_α}	Degradation rate of TNF-α	216.6 d^{-1}	[76]est.
μ_{T_β}	Degradation rate of TGF-β	495.1 d^{-1}	[85]est.
μ_V	Degradation rate of VEGF	16.5 d^{-1}	[86]est.
μ_w	Degradation rate of oxygen	$8.33 \times 10^{-3}\mathrm{d}^{-1}$	[87]est.
Continued			

Parameters	Descriptions	Values	References
μ_{M_1}	Death rate of M_1	0.033 d^{-1}	[78]est.
μ_{M_2}	Death rate of M_2	0.099 d^{-1}	[78]est.
μ_E	Death rate of endothelial cells	0.045 d^{-1}	[80]est.
μ_F	Death rate of F	0.02 d^{-1}	[88]est.
μ_{F_s}	Death rate of F_s	0.025 d^{-1}	est.
μ_{I_6}	Death rate of I_6	1.073 d^{-1}	[73]est.
μ_{PF}	Depletion rate of P by F	$1.043 \times 10^{-4}\mathrm{d}^{-1}$	est.
μ_{PM}	Depletion rate of P by M	$1.043 \times 10^{-4}\mathrm{d}^{-1}$	est.
μ_{EV}	Depletion rate of E by V	19.8 d^{-1}	est.
$\mu_{M_2 w}$	Depletion rate of M_2 by w	$9.9 \times 10^{-3}\mathrm{d}^{-1}$	est.
μ_{Fw}	Death rate of F by w	$2 \times 10^{-3}\mathrm{d}^{-1}$	est.
$\mu_{\rho Q}$	Rate of Q-enhanced secretion of ρ by F	5×10^{-3} d g^{-1}	est.
$\mu_{F_s Q}$	Rate of elimination of F_s by Q	$5 \times 10^{-2}\mathrm{g}^{-1}$	est.
D_{M_1}	Diffusion coefficient of M_1	$8.64 \times 10^{-7}\mathrm{cm}^2\mathrm{d}^{-1}$	[89]est.
D_{M_2}	Diffusion coefficient of M_2	$8.64 \times 10^{-7}\mathrm{cm}^2\mathrm{d}^{-1}$	[89]est.
D_E	Diffusion coefficient of E	$8.64 \times 10^{-7}\mathrm{cm}^2\mathrm{d}^{-1}$	[89]est.
D_F	Diffusion coefficient of F	$8.64 \times 10^{-7}\mathrm{cm}^2\mathrm{d}^{-1}$	[89]est.
D_{F_s}	Diffusion coefficient of F_s	$8.64 \times 10^{-7}\mathrm{cm}^2\mathrm{d}^{-1}$	[89]est.
D_P	Diffusion coefficient of P	$8.63 \times 10^{-2}\mathrm{cm}^2\mathrm{d}^{-1}$	[90]est.
D_{T_α}	Diffusion coefficient of T_α	$8.48 \times 10^{-2}\mathrm{cm}^2\mathrm{d}^{-1}$	[91]est.
D_{T_β}	Diffusion coefficient of T_β	$7.1 \times 10^{-2}\mathrm{cm}^2\mathrm{d}^{-1}$	[91]est.
D_V	Diffusion coefficient of V	$8.64 \times 10^{-2}\mathrm{cm}^2\mathrm{d}^{-1}$	[92]est.
D_w	Diffusion coefficient of w	2 $\mathrm{cm}^2\mathrm{d}^{-1}$	[93]est.
B_1	Diabetic effect of oxygen flow blockade	10	This work
B_2	Diabetic effect of $M_1 \to M_2$ blockade	2	This work
T_w	Diabetic effect of $M_1 \to M_2$ blockade	50 d	This work

Table 4. Parameters for the model.

Densities/concentrations in steady state

Estimate for ρ_0, ρ_m, ρ_1 and γ. The ECM density is 3–4% of the dry weight of tissue[61]; we accordingly take

$$\rho_0 = 0.04 \text{ g/cm}^3.$$

We also take

$$\rho_m = 1.1\rho_0 = 0.044 \text{ g/cm}^3, \ \rho_1 = 0.2\rho_0 = 0.008 \text{ g/cm}^3,$$

and

$$\gamma = 0.19 \text{ d}^{-1}.$$

Estimate for w_0.
The concentration of oxygen in tissue is given by the following formula (in text, section Materials and Methods of[62]):

$$w_0 = P_{O_2} \times \alpha_{tissue},$$

where $P_{O_2} = 100$ M/mmHg is the oxygen pressure in arterial blood and (from Table 3 in[62]) $\alpha_{tissue} = 1.25 \times 10^{-6}$ mmHg is the oxygen solubility in the tissue ($\mathrm{M} = 10^{-3}\frac{\mathrm{mol}}{\mathrm{cm}^3} = 32 \times 10^{-3}\frac{\mathrm{g}}{\mathrm{cm}^3}$). Hence

$$w_0 = 125 \times 10^{-6} \text{ M} = 4 \times 10^{-6} \text{ g/cm}^3.$$

F and M_2 cells undergo increased apoptosis as the oxygen concentration (in $\mathrm{g/cm}^3$) decreases from 4×10^{-6} to 3.2×10^{-7}. We assume that the rate of apoptosis is porportional to $D(w)$ and take

$$w_i = 2.5 \times 10^{-6} \text{ g/cm}^3.$$

Estimates for steady M_1^0 (of M_1) and M_2^0 (of M_2).
There are 2–4$\times 10^4$ macrophages per mm^3 in mid-dermis[63]. We take the number of macrophages to be 3×10^4 cells/mm^3 and the mass of a cell to be 5×10^{-10} g. We assume that $M_1^0 > M_2^0$ in the steady state of mid-epidermis, and take

$$M_1^0 = 2.5 \times 10^{-3}\ \mathrm{g/cm}^3,$$

and

$$M_2^0 = 5M_1^0 = 1.25 \times 10^{-2}\ \mathrm{g/cm}^3.$$

Estimate for F_0.
There are 2100–4100 fibroblasts/mm^3 in mid-dermis[64]. The volume of a fibroblast cell is 2.5×10^{-9} cm^3 [65](Fig. 1B) and accordingly we take its mass to be 2.5×10^{-9} g. Assuming that there are 3000 fibroblasts cells in mm^3, we get the steady-state of F to be

$$F_0 = 3 \times 10^6 \times 2.5 \times 10^{-9} = 7.5 \times 10^{-3}\ \mathrm{g/cm}^3.$$

Estimate for F_s^0
Wounds are hard to heal when the accumulation of senescent fibroblasts exceeds 15% threshold[66]. For diabetic wounds we take

$$F_s^0 = 40\%F_0 = 3 \times 10^{-3}\ \mathrm{g/cm}^3.$$

Estimate for E_0.
The number of human corneal endothelial cells is 3000 cells/mm^2, or 3×10^5 cells/cm^2[67,68]. We assume that the number of endothelial cells in mid-dermis is 2×10^7 cells/cm^3. Taking the mass of one cell to be 5×10^{-10} g, we get the steady-state of E:

$$E_0 = 2 \times 10^7 \times 5 \times 10^{-10} = 10^{-2}\ \mathrm{g/cm}^3.$$

Estimate for K_{I_6}
The level of IL-6 in normal human skin is approximately 205.1 pg/g[69](Tab. 1).

The level of IL-6 in human skin wounds is increasing after wound initiation[69](Fig. 4). We take the average level of IL-6 around the wound to be

$$K_{I_6} = 205.1 \times 2 = 4.102 \times 10^{-10}\ \mathrm{g/cm}^3.$$

Estimate for K_{T_β}
In humans, the level of TGF-β decreases from its high value within the first hours post wound initiation to reach an average of 100 pg/mm^3[70](Fig. 2).

Since diabetic wounds do not heal without intervention, we take

$$K_{T_\beta} = 100\ \mathrm{pg/mm}^3 = 10^{-7}\ \mathrm{g/cm}^3.$$

Estimate for K_P
In mice, the level of PDGF in the wound was measured to be approximately 6 ng/mg at day 3 post wound initiation and 1.5 ng/mg at day 7 post wound initiation[71](Fig. 2c).

We take in chronic wounds,

$$K_P = 4\ \mathrm{ng/mg} = 4 \times 10^{-6}\ \mathrm{g/cm}^3.$$

Estimate for K_V
We assume that the average level of VEGF after wound initiation is similar to that of murine skin 5 to 7 days after wound initiation[9](Fig. 7) and take

$$K_V = 1150\ \mathrm{pg/mg} = 1.15 \times 10^{-6}\ \mathrm{g/cm}^3.$$

Estimate for K_{T_α}
In murine skin, the level of TNF-α increases from its control level (60 pg/ml) to 120 pg/ml after wound initiation[72](Figs. 1,2). We take, in diabetic wounds,

$$K_{T_\alpha} = 100\ \mathrm{pg/ml} = 10^{-10}\ \mathrm{g/cm}^3.$$

Death/degradation rates
The death or degradation rate μ_X of a species X is linked to its half-life $t_{1/2}(X)$ by the formula:

$$\mu_X = \frac{\ln 2}{t_{1/2}(X)}.$$

Estimate for μ_{I_6}. The half-life of IL-6 is 15.5 hours[73], or equivalently 0.646 days. Hence,

$$\mu_{I_6} = 1.073 \text{ d}^{-1}.$$

Estimate for μ_P. The half-life of PDGF is 30 minutes[74]. We take $t_{1/2}(P) = 0.021$ days, so that

$$\mu_P = 33 \text{ d}^{-1}.$$

Estimate for μ_V. The half-life of VEGF is 60 minutes[75]. Hence $t_{1/2}(V) = 0.042$ days, and

$$\mu_V = 16.5 \text{ d}^{-1}.$$

Estimate for μ_{T_α}. The half-life of TNF-α is 4.6 minutes[76]. Hence $t_{1/2}(T_\alpha) = 3.2 \times 10^{-3}$ days, and

$$\mu_{T_\alpha} = 216.61 \text{ d}^{-1}.$$

Estimate for μ_{T_β}. The half-life of TGF-β is approximately 2 minutes[77]. Hence $t_{1/2}(T_\beta) = 1.4 \times 10^{-3}$ days, and

$$\mu_{T_\beta} = 495.1 \text{ d}^{-1}.$$

Estimate for μ_{M_1}. The half-life of tissue M1 macrophages is three weeks[78], or, equivalently, 21 days. Hence,

$$\mu_{M_1} = 0.033 \text{ d}^{-1}.$$

Estimate for μ_{M_2}. The half-life of tissue M2 macrophages is 7 days[78], so that

$$\mu_{M_2} = 0.099 \text{ d}^{-1}.$$

Estimate for μ_F and μ_{F_s}. The death rate of fibroblast is approximately 2.31×10^{-7} per second[79], hence,

$$\mu_F = 2.31 \times 10^{-7} \times 24 \times 60 \times 60 = 0.02 \text{ d}^{-1}.$$

We take

$$\mu_{F_s} = 1.25\mu_F = 0.025 \text{ d}^{-1}.$$

Estimate for μ_E. The half-life of cardiac endothelial cells is 2.2 weeks[80], or, equivalently, 15.4 days. Using the same half-life for dermal epithelial cells, we get

$$\mu_E = 0.045 \text{ d}^{-1}.$$

Chemotactic coefficients
We take

$$\chi_P = \chi_V = 1000 \text{ cm}^5/\text{g} \cdot \text{d},$$

which is in the range given in[81] for χ_P.

Estimates by equations
There are still many parameters that need to be estimated, including all the production coefficients. To do that we shall take, in each equation, its steady state, that is, make the right-hand side equal to zero, drop chemotactic terms, and replace each species by its steady state as estimated above.

Equation (3): From the steady state equation (3) in healthy tissue (i.e., with $T_\beta = 0$), we get

$$\lambda_\rho F(1 - \rho_0/\rho_m) = \mu_\rho \rho_0,$$

where $F = F_0 = 7.5 \times 10^{-3}$ g/cm^3, $\rho_m = 1.1\rho_0$, $\mu_\rho = 0.37 \text{ d}^{-1}$ by[36], and $\rho_0 = 0.04$ g/cm^3. Hence

$$\lambda_\rho = 21.71 \text{d}^{-1}.$$

We take

$$\lambda_{\rho T_\beta} = 0.1.$$

Equations (4) and (5): From the steady state equation (4) in healthy state, we get $A_{M_1} = \mu_{M_1} M_1^0$, where $\mu_{M_1} = 0.033\ \mathrm{d}^{-1}$ and $M_1^0 = 2.5 \times 10^{-3}\ \mathrm{g/cm}^3$. Hence,

$$A_{M_1} = 7.5 \times 10^{-5}\ \mathrm{g/cm}^3\,\mathrm{d}^{-1}.$$

We take $\lambda_{M_1P} = 0.2\mu_{M_1} = 6.6 \times 10^{-3}\ \mathrm{d}^{-1}$ and $\lambda_{M_1M_2} = \lambda_{M_1P}/2 = 3.3 \times 10^{-4}\ \mathrm{d}^{-1}$. We assume that $\lambda_{M_2M_1I_6} > \lambda_{M_1M_2T_\beta} > \lambda_{M_2M_1T_\alpha}$ and take $\lambda_{M_2M_1I_6} = 2\lambda_{M_1M_2T_\beta}$ and $\lambda_{M_1M_2T_\beta} = 11\lambda_{M_2M_1T_\alpha}$. Then from the steady state of Eq. (4)

$$A_{M_1} + \lambda_{M_1P} M_1^0/2 - 11\lambda_{M_2M_1T_\alpha} M_1^0/2 + \lambda_{M_2M_1T_\alpha} M_2^0/2 - \lambda_{M_1M_2} M_1^0 + \lambda_{M_2M_1T_\alpha} M_2^0/2 - \mu_{M_1} M_1^0 = 0$$

where $M_1^0 = 2.5 \times 10^{-3}\ \mathrm{g/cm}^3$ and $M_2^0 = 1.25 \times 10^{-2}\ \mathrm{g/cm}^3$, we get

$$\lambda_{M_1M_2T_\beta} = 5.94 \times 10^{-3}\ \mathrm{d}^{-1}, \lambda_{M_2M_1T_\alpha} = 6.53 \times 10^{-2}\ \mathrm{d}^{-1} \text{ and } \lambda_{M_2M_1I_6} = 5.94 \times 10^{-3}\ \mathrm{d}^{-1}.$$

All the coefficients in Eq. (5) are now estimated except μ_{M_2w}. We take

$$\mu_{M_2w} = \mu_{M_2}/10 = 9.9 \times 10^{-3}\ \mathrm{d}^{-1}.$$

Equation (6): We take $F_m = 2F_0 = 15 \times 10^{-3}\ \mathrm{g/cm}^3$ and $\lambda_{FF_s} = \lambda_F/10$. In steady state of health, $\lambda_F F(1 - F/F_m)/2 - \lambda_F F/10 - \mu_F F = 0$. Since $\mu_F = 0.02\ \mathrm{d}^{-1}$, we get

$$\lambda_F = 0.15\ \mathrm{d}^{-1} \text{ and } \lambda_{FF_s} = 0.015\ \mathrm{d}^{-1}.$$

We take

$$\mu_{Fw} = \mu_F/10 = 2 \times 10^{-3}\ \mathrm{d}^{-1}.$$

Equation (8): We take $\lambda_{EV} = 1$. Then the steady state reduces to $3\lambda_E/2 - \mu_E E_0 = 0$, where $\mu_E = 0.045\ \mathrm{d}^{-1}$ and $E_0 = 10^{-2}\ \mathrm{g/cm}^3$, so that

$$\lambda_E = 3 \times 10^{-4}\ \mathrm{g/cm}^3\,\mathrm{d}^{-1}.$$

Equation (9): We take the "average" value of $R(t)$ in diabetic wounds control case to be $\bar{R} = 0.7$ cm, and assume that $\lambda_P \bar{R} - \mu_P K_P = 0$, so that

$$\lambda_P = 1.19 \times 10^{-4}\ \mathrm{g/cm}^3\,\mathrm{d}^{-1}.$$

Next, in steady-state, $\lambda_{FP} F = (\mu_{PF} F + \mu_{PM} M_1)/2$. We assume that $\mu_{PF} = \mu_{PM} = \theta\lambda_P$ for some $\theta > 0$. Taking $\theta = 1.23$, we get $\lambda_P + \lambda_{FP} F - \mu_{PF}(F + M_1)/2 - \mu_P K_P = 0$. Hence,

$$\mu_{PF} = \mu_{PM} = 1.043 \times 10^{-4}\ \mathrm{d}^{-1}, \text{ and } \lambda_{FP} = 7 \times 10^{-5}\ \mathrm{d}^{-1}.$$

Equation (10): The steady state equation is $\lambda_{M_1T_\alpha} M_1^0 - \mu_{T_\alpha} K_{T_\alpha} = 0$, where $M_1^0 = 2.5 \times 10^{-3}\ \mathrm{g/cm}^3$, $K_{T_\alpha} = 10^{-10}\ \mathrm{g/cm}^3$ and $\mu_{T_\alpha} = 216.6\ \mathrm{d}^{-1}$. Hence,

$$\lambda_{M_1T_\alpha} = 8.664 \times 10^{-6}\ \mathrm{d}^{-1}.$$

Equation (11): We take $\lambda_{FT_\beta} = \lambda_{M_2T_\beta}$. The steady state equation then becomes $\lambda_{FT_\beta}(M_2^0 + F_0) - \mu_{T_\beta} K_{T_\beta} = 0$, where $M_2^0 = 1.25 \times 10^{-2}\ \mathrm{g/cm}^3$, $F_0 = 7.5 \times 10^{-3}\ \mathrm{g/cm}^3$, $K_{T_\beta} = 10^{-7}\ \mathrm{g/cm}^3$, and $\mu_{T_\beta} = 495.1\ \mathrm{d}^{-1}$. Hence,

$$\lambda_{FT_\beta} = \lambda_{M_2T_\beta} = 2.5 \times 10^{-3}\ \mathrm{d}^{-1}.$$

Equation (12): The steady-state is given by $\lambda_{F_sI_6} F_s^0 - \mu_{I_6} K_{I_6} = 0$, where $F_s^0 = 3 \times 10^{-3}\ \mathrm{g/cm}^{-3}$, $K_{I_6} = 4.102 \times 10^{-10}\ \mathrm{g/cm}^{-3}$, and $\mu_{I_6} = 1.073\ \mathrm{d}^{-3}$. Hence,

$$\lambda_{F_sI_6} = 2.9343 \times 10^{-7}\ \mathrm{d}^{-1}.$$

Equation (13): F_s secretes significantly more VEGF than F[40,41]. We take $\lambda_{F_sV} = 10\lambda_{FV}$, $\lambda_{FV} = \lambda_{M_2V}$, $\mu_{EV} = 1.2\mu_V$, and write the time-average steady-state with the av-

erage value of $A(t)$ over 30 days, $\bar{A} = \frac{1}{30}\int_0^{30} \frac{A_0}{1+t^2/T_w^2}$ with $A_0 = 0.5$ and $T_w = 50$ d, as follows: $(\lambda_{FV}F_0 + 10\lambda_{FV}F_s^0)\bar{A} + \lambda_{FV}M_2^0 - 1.2\mu_V E_0/2 - \mu_V K_V = 0$, where $M_2^0 = 1.25 \times 10^{-2}$ g/cm^{-3}, $E_0 = 10^{-2}$ g/cm^{-3}, $K_V = 1.15 \times 10^{-6}$ g/cm^3, $\mu_V = 16.5$ d^{-1} and $\bar{A} = 0.45035$. Hence,

$$\lambda_{FV} = 3.17 \text{ d}^{-1},\ \lambda_{F_sV} = 31.7 \text{ d}^{-1},\ \lambda_{M_2V} = 3.17 \text{ d}^{-1} \text{ and } \mu_{EV} = 19.8 \text{ d}^{-1}.$$

Equation (15): From the steady state in health, $\lambda_{Ew}E_0 - c_w(F_0 + M_2^0)w_0 = 0$, where $E_0 = 10^{-2}$ g/cm^{-3}, $F_0 = 7.5 \times 10^{-3}$ g/cm^3, $M_2^0 = 1.25 \times 10^{-2}$ g/cm^3 and $w_0 = 4 \times 10^{-6}$ g/cm^3. Hence,

$$\lambda_{Ew} = 8 \times 10^{-6} \times c_w \text{ d}^{-1}.$$

Taking

$$c_w = 0.3 \text{ cm}^3/\text{g d}^{-1},\ \text{we get } \lambda_{Ew} = 2.4 \times 10^{-6} \text{ d}^{-1}.$$

Data availability

All data generated or analyzed during this study are included in this published article.

Received: 28 February 2025; Accepted: 16 May 2025
Published online: 23 May 2025

References

1. Kwan, P. O. & Tredget, E. E. Biological principles of scar and contracture. *Hand Clin.* **33**(2), 277–292 (2017).
2. Sadeghi-Ardebili, M., Hasannia, S., Dabirmanesh, B. & Khavari-Nejad, R. A. Functional characterization of the dimeric form of PDGF-derived fusion peptide fabricated based on theoretical arguments. *Sci. Rep.* **14**(1), 1003 (2024).
3. Wilgus, T. A., Roy, S. & McDaniel, J. C. Neutrophils and wound repair: Positive actions and negative reactions. *Adv. Wound Care (New Rochelle).* **2**(7), 379–388 (2013).
4. Krzyszczyk, P., Schloss, R., Palmer, A. & Berthiaume, F. The role of macrophages in acute and chronic wound healing and interventions to promote pro-wound healing phenotypes. *Front. Physiol.* **9**, 419 (2018).
5. Lu, H. L. et al. Activation of M1 macrophages plays a critical role in the initiation of acute lung injury. *Biosci. Rep.* **38**(2), BSR20171555 (2018).
6. Ramirez, H., Patel, S. B. & Pastar, I. The role of TGF-β signaling in wound epithelialization. *Adv. Wound Care (New Rochelle)* **3**(7), 482–491 (2014).
7. Zhang, F. et al. TGF-β induces M2-like macrophage polarization via SNAIL-mediated suppression of a pro-inflammatory phenotype. *Oncotarget* **7**(32), 52294–52306 (2016).
8. Wu, X. et al. TNF-α mediated inflammatory macrophage polarization contributes to the pathogenesis of steroid-induced osteonecrosis in mice. *Int. J. Immunopathol. Pharmacol.* **28**(3), 351–361 (2015).
9. Johnson, K. E. & Wilgus, T. A. Vascular endothelial growth factor and angiogenesis in the regulation of cutaneous wound repair. *Adv. Wound Care* **3**(10), 647–661 (2014).
10. Shibuya, M. Vascular endothelial growth factor (VEGF) and its receptor (VEGFR) signaling in angiogenesis: A crucial target for anti- and pro-angiogenic therapies. *Genes Cancer* **2**(12), 1097–1105 (2011).
11. Liarte, S. & Nicolás, A. B. F. J. Role of TGF-β in skin chronic wounds: A keratinocyte perspective. *Cells* **9**(2), 306 (2020).
12. Alam, W., Hasson, J. & Reed, M. Clinical approach to chronic wound management in older adults. *J. Am. Geriatr. Soc.* **69**(8), 2327–2334 (2021).
13. Gould, L. et al. Chronic wound repair and healing in older adults: Current status and future research. *J. Am. Geriatr. Soc.* **63**(3), 427–438 (2015).
14. Elder, S. S. & Emmerson, E. Senescent cells and macrophages: Key players for regeneration?. *Open Biol.* **10**(12), 200309 (2020).
15. Wei, X. et al. Senescence in chronic wounds and potential targeted therapies. *Burns Trauma* **10**, tkab045 (2022).
16. Andrade, A. M. et al. Role of senescent cells in cutaneous wound healing. *Biology (Basel)* **11**(12), 1731 (2022).
17. Hou, J. & Kim, S. Possible role of ginsenoside Rb1 in skin wound healing via regulating senescent skin dermal fibroblast. *Biochem. Biophys. Res. Commun.* **499**(2), 381–388 (2018).
18. Johnson, B. Z., Stevenson, A. W., Prêle, C. M., Fear, M. W. & Wood, F. M. The role of IL-6 in skin fibrosis and cutaneous wound healing. *Biomedicines* **8**(5), 101 (2020).
19. Wilkinson, H. N. & Hardman, M. J. Senescence in wound repair: Emerging strategies to target chronic healing wounds. *Front. Cell Dev. Biol.* 8 (2020).
20. Chin, T., Lee, X. E., Ng, T. Y., Lee, Y. & Dreesen, O. The role of cellular senescence in skin aging and age-related skin pathologies. *Front. Physiol.* **14**, 1297637 (2023).
21. Zhang, J., Yu, H., Man, M. Q. & Hu, L. Aging in the dermis: Fibroblast senescence and its significance. *Aging Cell* **23**(2), e14054 (2024).
22. Varani, J. et al. Vitamin A antagonizes decreased cell growth and elevated collagen-degrading matrix metalloproteinases and stimulates collagen accumulation in naturally aged human skin. *J. Invest. Dermatol.* **114**(3), 480–486 (2000).
23. Pulido, T., Velarde, M. C. & Alimirah, F. The senescence-associated secretory phenotype: Fueling a wound that never heals. *Mech. Ageing Dev.* **199**, 111561 (2021).
24. Wu, X. et al. Macrophage polarization in diabetic wound healing. *Burns Trauma* **10**, tkac051 (2022).
25. Lähteenvuo, J. & Rosenzweig, A. Effects of aging on angiogenesis. *Circ. Res.* **110**(9), 1252–64 (2012).
26. Xiao, P. et al. Impaired angiogenesis in ageing: The central role of the extracellular matrix. *J. Transl. Med.* **21**(1), 457 (2023).
27. Fujisaka, S. The role of adipose tissue M1/M2 macrophages in type 2 diabetes mellitus. *Diabetol. Int.* **12**(1), 74–79 (2020).
28. Catrina, S. B. & Zheng, X. Hypoxia and hypoxia-inducible factors in diabetes and its complications. *Diabetologia* **64**(4), 709–716 (2021).
29. Sano, H. & Ichioka, S. Topical wound oxygen therapy for chronic diabetic lower limb ulcers and sacral pressure ulcers in Japan. *Case Rep. Wounds Int.* **6**(1) (2015).
30. Spiliopoulos, S., Festas, G., Paraskevopoulos, I., Mariappan, M. & Brountzos, E. Overcoming ischemia in the diabetic foot: Minimally invasive treatment options. *World J. Diabetes* **12**(12), 2011–2056 (2021).
31. Sharma, R., Sharma, S. K., Mudgal, S. K., Jelly, P. & Thakur, K. Efficacy of hyperbaric oxygen therapy for diabetic foot ulcer, a systematic review and meta-analysis of controlled clinical trials. *Sci. Rep.* **11**, 2189 (2021).

32. Hanley, M. E. & Manna, B. Hyperbaric Treatment of Diabetic Foot Ulcer. StatPearls [Internet] Treasure Island (FL): StatPearls Publishing (2024).
33. Zulkefli, N. et al. Flavonoids as potential wound-healing molecules: Emphasis on pathways perspective. *Int. J. Mol. Sci.* **24**(5), 4605 (2023).
34. Chittasupho, C., Manthaisong, A., Okonogi, S., Tadtong, S. & Samee, W. Effects of quercetin and curcumin combination on antibacterial, antioxidant, in vitro wound healing and migration of human dermal fibroblast cells. *Int. J. Mol. Sci.* **23**(142) (2022).
35. Friedman, A. & Siewe, N. Overcoming drug resistance to BRAF inhibitor. *Bull. Math. Biol.* **82**(8) (2020).
36. Xue, C., Friedman, A. & Sen, C. K. A mathematical model of ischemic cutaneous wounds. *Proc. Nat. Acad. Sci.* **106**, 16782–16787 (2009).
37. Mouton, A. J. et al. Mapping macrophage polarization over the myocardial infarcation time continuum. *Basic Res. Cardiol.* **113**(4), 26 (2018).
38. Kramer, P. A., Ravi, S., Chacko, B., Johnson, M. S. & Darley-Usmar, V. M. A review of the mitochondrial and glycolytic metabolism in human platelets and leukocytes: Implications for their use as bioenergetic biomarkers. *Redox Biol.* **2**, 206–210 (2014).
39. Pierce, G. F., Mustoe, T. A., Altrock, B. W., Deuel, T. F. & Thomason, A. Role of platelet-derived growth factor in wound healing. *J. Cell Biochem.* **45**(4), 319–326 (1991).
40. Xiao, Y. et al. Senescent cells with augmented cytokine production for microvascular bioengineering and tissue repairs. *Adv. Biosyst.* **3**(8), 1900089 (2019).
41. Coppé, J. P., Desprez, P. Y., Krtolica, A. & Campisi, J. The senescence-associated secretory phenotype: The dark side of tumor suppression. *Annu. Rev. Pathol.* **5**, 99–118 (2010).
42. Chaib, S., Tchkonia, T. & Kirkland, J. L. Cellular senescence and senolytics: The path to the clinic. *Nat. Med.* **28**, 1556–1568 (2022).
43. Mi, Y. et al. Quercetin promotes cutaneous wound healing in mice through Wnt/β-catenin signaling pathway. *J. Ethnopharmacol.* **23**(290), 115066 (2022).
44. Hwang, H. V., Tran, D. T., Rebuffatti, M. N., Li, C. S. & Knowlton, A. A. Investigation of quercetin and hyperoside as senolytics in adult human endothelial cells. *PLoS One* **13**(1), e0190374 (2018).
45. Pang, X. G., Cong, Y., Bao, N. R., Li, Y. G. & Zhao, J. N. Quercetin stimulates bone marrow mesenchymal stem cell differentiation through an estrogen receptor-mediated pathway. *BioMed Res. Int.* **2018**(4178021), 1–11 (2018).
46. Islam, M. T. et al. Senolytic drugs, dasatinib and quercetin, attenuate adipose tissue inflammation, and ameliorate metabolic function in old age. *Aging Cell* **22**(2), e13767 (2023).
47. Lee, E. et al. Exploring the effects of Dasatinib, Quercetin, and Fisetin on DNA methylation clocks: A longitudinal study on senolytic interventions. *Aging (Albany NY)* **16**(4), 3088–3106 (2024).
48. Hickson, L. et al. Senolytics decrease senescent cells in humans: Preliminary report from a clinical trial of Dasatinib plus Quercetin in individuals with diabetic kidney disease. *EBioMedicine* **47**, 446–456 (2019).
49. Huang, H., Chen, Y., Hu, J., Guo, X., Zhou, S., Yang, Q., et al. Quercetin and its derivatives for wound healing in rats/mice: Evidence from animal studies and insight into molecular mechanisms. *Int. Wound J.* **21** (2023).
50. Abid, H. M. U. et al. Wound-Healing and Antibacterial Activity of the Quercetin-4-Formyl Phenyl Boronic Acid Complex against Bacterial Pathogens of Diabetic Foot Ulcer. *ACS Omega.* **7**(28), 24415–14432 (2022).
51. Spampinato, S. F., Caruso, G. I., De Pasquale, R., Sortino, M. A. & Merlo, S. The treatment of impaired wound healing in diabetes: Looking among old drugs. *Pharmaceuticals (Basel)* **13**(4), 60 (2020).
52. Oyebode, O. A., Jere, S. W. & Houreld, N. N. Current therapeutic modalities for the management of chronic diabetic wounds of the foot. *J. Diabetes Res.* **2023**(10), 1359537 (2023).
53. Raghav, A. et al. Financial burden of diabetic foot ulcers to world: A progressive topic to discuss always. *Ther. Adv. Endocrinol. Metab.* **9**(1), 29–31 (2018).
54. Hicks, C. W. et al. Burden of infected diabetic foot ulcers on hospital admissions and costs. *Ann. Vasc. Surg.* **33**, 149–158 (2016).
55. Kerr, M. et al. The cost of diabetic foot ulcers and amputations to the National Health Service in England. *Diabet Med.* **36**(8), 995–1002 (2019).
56. Tchero, H. et al. Cost of diabetic foot in France, Spain, Italy, Germany and United Kingdom: A systematic review. *Ann. Endocrinol. (Paris)* **79**(2), 67–74 (2018).
57. Zhang, G. et al. Revolutionizing diabetic foot ulcer care: The senotherapeutic approach. *Aging Dis.* **16**(2), 946–970 (2024).
58. Pouwer, F. et al. The quest for wellness: How to optimise self-care strategies for diabetic foot management?. *Diabetes Metab. Res. Rev.* **40**(3), e3751 (2024).
59. Kirschner, D. E. Uncertainty and sensitivity functions and implementation. http://malthus.micro.med.umich.edu/lab/usadata/: University of Michigan; 2007–2008.
60. Marino, S., Hogue, I. B., Ray, C. J. & Kirschner, D. E. A methodology for performing global uncertainty and sensitivity analysis in systems biology. *J. Theor. Biol.* **254**, 178–196 (2008).
61. Xue, M. & Jackson, C. J. Extracellular matrix reorganization during wound healing and its impact on abnormal scarring. *Adv. Wound Care* **4**(3), 119–136 (2015).
62. Beard, D. A. Modeling of oxygen transport and cellular energetics explains observations on in vivo cardiac energy metabolism. *PLoS Comput. Biol.* **2**(9), e107 (2006).
63. Tong, P. L. et al. The skin immune atlas: Three-dimensional analysis of cutaneous leukocyte subsets by multiphoton microscopy. *J. Invest. Dermatol.* **135**(1), 84–93 (2015).
64. Miller, C. C. et al. Validation of a morphometric method for evaluating fibroblast numbers in normal and pathologic tissues. *Exp. Dermatol.* **12**(4), 403–11 (2003).
65. Padovan-Merhar, O. et al. Single mammalian cells compensate for differences in cellular volume and DNA copy number through independent global transcriptional mechanisms. *Mol. Cell* **58**(2), 339–352 (2015).
66. Harding, K. G., Moore, K. & Phillips, T. J. Wound chronicity and fibroblast senescence-implications for treatment. *Int. Wound J.* **2**(4), 364–368 (2005).
67. Bourne, W. M. Biology of the corneal endothelium in health and disease. *Eye* **17**, 912–918 (2003).
68. Kim, J. A. et al. TSG-6 protects corneal endothelium form transcorneal cryoinjury in rabbits. *Invest. Ophthalmol. Vis. Sci.* **55**, 4905–4912 (2014).
69. Grellner, W., Georg, T. & Wilske, J. Quantitative analysis of proinflammatory cytokines (IL-1beta, IL-6, TNF-alpha) in human skin wounds. *Forensic Sci. Int.* **113**(1–3), 251–264 (2000).
70. Yang, L., Qiu, C. X., Ludlow, A., Ferguson, M. W. & Brunner, G. Active transforming growth factor-beta in wound repair: Determination using a new assay. *Am. J. Pathol.* **154**(1), 105–111 (1999).
71. White, M. J. V., Briquez, P. S., White, D. A. V. & Hubbell, J. A. VEGF-A, PDGF-BB and HB-EGF engineered for promiscuous super affinity to the extracellular matrix improve wound healing in a model of type 1 diabetes. *NPJ Regen. Med.* **6**(1), 76 (2021).
72. Ritsu, M. et al. Critical role of tumor necrosis factor-α in the early process of wound healing in skin. *J. Dermatol. Dermatol. Surg.* **21**(1), 14–19 (2017).
73. Kuribayashi, T. Elimination half-lives of interleukin-6 and cytokine-induced neutrophil chemoattractant-1 synthesized in response to inflammatory stimulation in rats. *Lab. Anim. Res.* **34**(2), 80–83 (2018).
74. Saik, J. E., Gould, D. J., Watkins, E. M., Dickinson, M. E. & West, J. L. Covalently immobilized platelet-derived growth factor-BB promotes angiogenesis in biomimetic poly(ethylene glycol) hydrogels. *Acta Biomater.* **7**(1), 133–143 (2011).

75. Finley, S. D., Engel-Stefanini, A. O., Imoukhuede, P. & Popel, A. S. Pharmacokinetics and pharmacodynamics of VEGF-neutralizing antibodies. *BMC Syst. Biol.* **5**(193), 1–20 (2011).
76. Simo, R., Barbosa-Desongles, A., Lecube, A., Hernandez, C. & Selva, D. M. Potential role of tumor necrosis factor-α in downregulating sex hormone-binding globulin. *Diabetes* **61**, 372–382 (2012).
77. Kaminska, B., Wesolowska, A. & Danilkiewicz, M. TGF beta signaling and its role in tumour pathogenesis. *Acta Biochim. Pol.* **52**(2), 329–337 (2005).
78. Italiani, P. & Boraschi, D. From monocytes to M1/M2 macrophages: Phenotypical vs. functional differentiation. *Front. Immunol.* **5**(514), 1–22 (2014).
79. Cohen, I. K., Die-gelmann, R. F. & Lindblad, W. J. Wound healing: Biochemical & clinical apects. *Plast. Reconstr. Surg.* **90**(5), 926 (1992).
80. Erben, R. G., Odorfer, K. I., Siebenhutter, M., Weber, K. & Rohleder, S. Histological assessment of cellular half-life in tissues in vivo. *Histochem. Cell Biol.* **130**, 1041–1046 (2008).
81. Ford, R. M. & Lauffenburger, D. A. Measurement of bacterail random motility and chemotaxis coefficients: II. Application of single-cell-based mathematical model. *Biotech. Bioeng.* **37**, 661–672 (1991).
82. Boron, W. F. & Boulpaep, E. L. *Medical Physiology: A Cellular and Molecular Approach* 2nd edn. (Sounders, Elsevier, 2012).
83. Berman, H. M. et al. The protein data bank. *Nucleic Acids Res.* **28**(1), 235–242 (2012).
84. Gay, C. G. & Winkles, J. A. The half-lives of platelet-derived growth factor a-and b-chain MRNAS are similar in endothelial cells and unaffected by heparin-binding growth factor-1 or cycloheximide. *J. Cell. Physiol.* **147**(1), 121–127 (1991).
85. Fuentes-Calvo, C. Atlas of genetics and cytogenetics in oncology and haematology. URL: http://atlasgeneticsoncologyorg/.
86. Shima, D. T., Deutsch, U. & D'Amore, P. A. Hypoxic induction of vascular endothelial growth factor (VEGF) in human epithelial cells is mediated by increases in MRNA stability. *FEBS Lett.* **370**(3), 203–208 (1995).
87. Troester, M. A., Lindstrom, A. B., Kupper, L. L. & Rappaport, S. W. S. M. Stability of hemoglobin and albumin adducts of benzene oxide and 1,4-benzoquinone after administration of benzene to F344 rats. *Toxicol. Sci.* **54**(1), 88–94 (2000).
88. Weissman-Shomer, P. & Fry, M. Chick embryo fibroblasts senscence in vitro: Pattern of cell division and life span as a function of cell density. *Mech. Ageing Dev.* **4**(2), 159–166 (1975).
89. Hao, W., Crouser, E. D. & Friedman, A. Mathematical model of sarcoidosis. *PNAS* **111**(45), 16065–16070 (2014).
90. PROSPEC: Protein Specialists. PDGF BB Human. URL: https://wwwprospecbiocom/pdgf-bb_human. Accessed April 19, 2019.
91. Hornbeck, P. V. et al. PhosphoSitePlus, 2014: Mutations, PTMs and recalibrations. *Nucleic Acids Res.* **43**, D512–D520 (2015).
92. Liao, K. L., Bai, X. F. & Friedman, A. Mathematical modeling of interleukin-27 induction of anti-tumor T cells response. *PLoS ONE* **9**(3) (2014).
93. Androjna, C., Gatica, J. E., Belovich, J. M. & Derwin, K. A. Oxygen diffusion through natural extracellular matrices: Implications for estimating "critical thickness" values in tendon tissue engineering. *Tissue Eng. Part A* **14**(4), 559–569 (2008).

Acknowledgements

Research reported in this publication was supported by the National Institute Of General Medical Sciences of the National Institutes of Health under Award Number R16GM154782. The content is solely the responsibility of the authors and does not necessarily represent the official views of the National Institutes of Health.

Additional information

Correspondence and requests for materials should be addressed to N.S.

Reprints and permissions information is available at www.nature.com/reprints.

Publisher's note Springer Nature remains neutral with regard to jurisdictional claims in published maps and institutional affiliations.